Acta Acustica 2024, **8**, 54

https://doi.org/10.1051/aacus/2024046

Topical Issue – Vibroacoustics

Available online at:
https://acta-acustica.edpsciences.org

SCIENTIFIC ARTICLE OPEN ACCESS

Structure-property relationships of polydisperse open-cell foams: Application to melamine foams

Cong Truc Nguyen[1,2], Dengke Li[1,3], Ziming Xiong[1,4], Mu He[1,5], Laurent Gautron[6], Arnaud Duval[2], and Camille Perrot[1,*]

[1] Univ Gustave Eiffel, Univ Paris Est Creteil, CNRS, UMR 8208, MSME, 77454 Marne-la-Vallée, France
[2] TREVES Products, Services & Innovation, 2-4 rue Emile Arquès - CS 70017 - 51686 Reims Cedex 2, France
[3] The State Key Laboratory of Heavy-duty and Express High-power Electric Locomotive, Zhuzhou 412001, Hunan Province, China
[4] LMEE Univ-Evry, Université Paris-Saclay, 91020 Evry, France
[5] Huazhong University of Science and Technology, No.1037 Luoyu Road, Wuhan 430074, China
[6] Univ Gustave Eiffel, CNRS, EA 4508, LGE, 77454 Marne-la-Vallée, France

Received 28 February 2024, Accepted 29 July 2024

Abstract – Melamine foam, categorized as an open-cell foam structure, absorbs sound through its three-dimensional network of thin struts. The pore size polydispersity within the open-cell melamine microstructure is evidenced from a top-down approach and confirmed by scanning electron microscope (SEM)-image analysis. The remarkable ability of melamine foams to mitigate sound energy is attributed to the pore size distribution, which encompasses co-existing pores of distinct characteristic sizes. Consequently, low-frequency and high-frequency fluid flows will follow different paths within the pore structure. A poly-sized model, which provides a connection between microstructure polydispersity and macroscopic properties, is successfully applied to three different melamine foams. This work highlights the significance and implications of polydispersity effects on the acoustic behavior of open-cell foams.

Keywords: Melamine foams, Acoustic behavior, Polydispersity effect, Micro-macro model

1 Introduction

The melamine resin foam is produced by foaming a resin composed of a melamine-formaldehyde condensate with a blowing agent [1]. These melamine foams present a unique microstructure characterized by an interconnected network of solid struts which form the edges and faces of open cells (Fig. 1), with struts of length L and thickness t so long and thin ($t \ll L$) that its porosity ϕ (fluid volume fraction) is not far from unity ($\phi \approx 0.99$, $\phi \to 1$). At the microscopic level (Fig. 1), Plateau's rules [2] describe the local structure of a liquid foam, the precursor of a solid foam. Cell faces always meet in threes along an edge or strut called a Plateau border, and they do so at an angle of $\arccos(-1/2) = 120°$ (for three bubbles). These Plateau borders meet in fours at a vertex or node, at an angle of $\arccos(-1/3) \approx 109.47°$ (the tetrahedral angle). In a typical melamine foam, the microstructure consists of struts of ligaments having concave-triangular cross-section, Magnet et al. provided a estimate of the struts diameter and length, which were found to be on the order of 5 µm and 100 µm, respectively [3]. The results of Plateau's rules apply to idealizations of many solid foam struts which are governed by surface tension such as aggregates of cells found in melamine foam, and which minimize surface area (Surface Evolver software [4]).

A sound wave impinging the surface of a melamine foam is partly reflected, and partly absorbed, through visco-thermal dissipation when penetrating into the porous material backed by a rigid wall. At the macroscopic scale, an effective medium approximation characterizing the visco-thermal losses, that is experimentally viable, requires only the determination of two frequency-dependent response functions, $k(\omega)$ and $k'(\omega)$. Here, $k(\omega)$ and $k'(\omega)$ are, respectively, the dynamic viscous permeability and the dynamic thermal permeability. In their original paper on the dynamic viscous permeability of a porous medium, Johnson et al. [5] proposed a fit for $k(\omega)$ relying on rigorous mathematical foundations that involves three parameters k_0, α_∞ and Λ; where k_0 is the static viscous permeability, α_∞ is the tortuosity and Λ is the viscous characteristic length. The expression for the dynamic thermal permeability, $k'(\omega)$, was given similarly by Champoux and Allard [6] and Lafarge et al. [7], involving the static thermal permeability k_0' and the thermal characteristic length Λ'. The dynamic viscous $k(\omega)$ and thermal $k'(\omega)$ permeabilities as provided through these models [5–7] are also often referred to as the

*Corresponding author: camille.perrot@univ-eiffel.fr

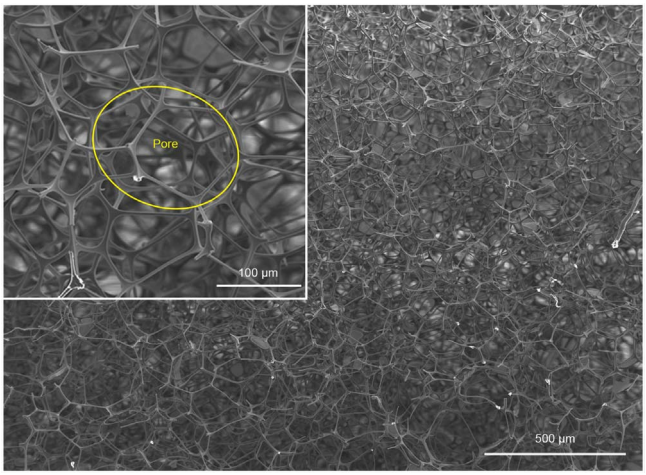

Figure 1. (Color online) Scanning electron microscope (SEM) image of a melamine foam sample (G+).

Johnson-Champoux-Allard-Lafarge or JCAL model. An experimental procedure [8, 9], which requires direct measurements of ϕ and k_0 and three-microphone impedance tube technique [10], provides a means to identify experimental values of α_∞, Λ, Λ' and k_0'; see also Ref. [11] (Tab. I) and Ref. [12] (Sect. 6.2) for complementary characterization techniques involving either elastic properties or anisotropic behavior. However, an experimental study of this nature would not help to relate directly visco-thermal dissipation to geometrical parameters of the porous structure, without specific attention at the microscopic level.

When a sound wave propagates through an air saturated porous media having a motionless and isothermal skeleton, the frequency-dependent interplay between viscosity and inertia, and thermal conduction produces a spatial gradient of fluid velocity and temperature; and the shear combined with heat transfer between successive layers of fluid causes compression wave attenuation. The characteristic lengths of the compression waves created by an oscillating body in which the main visco-inertial and thermal dissipation processes occur, are the viscous and thermal boundary layers. They scale, respectively, as $\delta_v = \sqrt{\nu/\omega}$ and $\delta_t = \sqrt{\nu'/\omega}$, in which $\nu = \eta/\rho_0$ is the fluid's cinematic viscosity, $\nu' = \kappa/(\rho_0 C_p)$ is its thermal diffusivity, ω is the angular frequency of motion; and where η is the fluid's dynamic viscosity, ρ_0 is its density at rest, κ is its thermal conductivity, C_p is the specific heat at constant pressure. For small perturbations, because the wavelength λ of the incident compression wave greatly exceeds the typical pore size D of the motionless porous media at audible frequencies, visco-inertial motions and thermal conduction can be decoupled within a pore. On the other hand, the elastic behavior of the solid matrix may be subsequently incorporated as an additional pressure source term for the fluid flow. The viscous forces at low frequencies (Stokes flow), inertial forces at high frequencies (potential flow formally identical to electric conduction), and thermal conduction at low frequencies (similar to diffusion-controlled reactions) together determine all the transport parameters within a porous material. For further details on the asymptotic behavior and the corresponding equations, see, for instance, Refs. [13, 14].

Real foams like melamine foams exhibit a random distribution of pore sizes (see Figs. 1 and 3). Despite this variability, the relationships between the pore size variation of open-cell foams (micro-structure) and their acoustic properties (macro-behavior) have received limited attention. In the present work, we aim to examine the applicability of acoustic micro-macro models to commercially available melamine foam samples, leveraging either measured macroscopic properties (top-down approach) or characterized microstructural features (bottom-up approach) as input parameters. Our objective is to demonstrate that the polydisperse feature of melamine foam has to be taken into account to provide a comprehensive picture of this acoustic material at both micro- and macro-scales.

2 Downscaling approach: Evidence of polydispersity

In 1887, Lord Kelvin proposed that the tetrakaidecahedron was the best shape for packing equal-sized objects together to fill space [15]. A Kelvin-cell structure consisting of 14 faces (six squared faces and eight hexagonal faces) is widely employed to describe the transport and acoustic properties of open-cell foam [13, 16–18]. Particularly, Perrot et al. [13] introduced a downscaling approach to simulate the acoustic properties of open-cell foams. In their approach, the measured viscous permeability k_0 and open porosity were used to determine the size of an approximate Kelvin cell, while the remaining transport parameters were derived through simulations on the determined Kelvin cell. In this section, we extend this top-down multi-scale approach for all transport parameters (of the JCAL model) and further analyze the resulting Kelvin-cell pore sizes by comparison with measurements carried out from scanning electron microscope (SEM) images.

In Langlois et al. [17], numerical simulations of viscous fluid, potential flows and thermal conduction were performed on the body centered cubic (BCC) structure using the Surface Evolver and finite element method. The visco-thermal parameters of open-cell monodisperse foams were calculated with several solid volume fractions. For low solid volume fraction ($1 - \phi \leq 0.11$), the bcc structure corresponds to the so-called Kelvin structure with Plateau borders, as illustrated in Figure 2. Based on the simulation data, approximate formulas were proposed for the transport parameters of open-cell foam materials:

$$k_0^* \approx \exp(-68.617x^5 + 148.54x^4 - 124.36x^3 + 49.897x^2 - 13.701x - 3.532), \quad (1)$$

$$k_0'^* \approx \frac{1}{60}\left(-0.68\ln x + 0.48 - \phi_s + 0.7x - 0.18x^2\right), \quad (2)$$

$$\Lambda^* \approx \left(0.087x^{1.16}(1-x)^{0.37} + 0.065x^{0.37}(1-x)^{1.16}\right)x^{-1}, \quad (3)$$

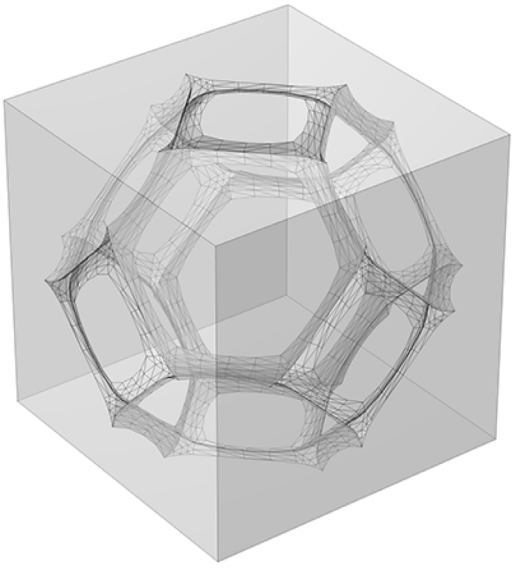

Figure 2. An illustration of the Kelvin-cell structure with Plateau borders obtained using the Surface Evolver software [4]. The Plateau borders result in a concave triangular cross-section of the ligaments, mimicking the structure observed in real melamine microstructures (refer to the inset of Fig. 1).

$$\Lambda'^{*} \approx \frac{1}{3}\left(-0.85x^{0.94} + 1.85x^{0.5}\right)^{-1}, \tag{4}$$

$$\alpha_{\infty}^{*} \approx \phi\left(0.47(1-x)^{2.47} + 0.53(1-x)^{0.5}\right)^{-1}, \tag{5}$$

where $x = (1-\phi)/\phi_s$ with ϕ_s a critical solid volume fraction. The superscript "*" denotes the transport parameter normalized by the average pore size D with the appropriate exponent: $k_0^* = k_0/D^2$, $k_0'^* = k_0'/D^2$, $\Lambda^* = \Lambda/D$ and $\Lambda'^* = \Lambda'/D$. In particular, $\alpha_{\infty}^* = \alpha_{\infty}$ because the tortuosity is dimensionless and scale-invariant. More specifically, the *normalized* transport parameters represent the values obtained from the Kelvin-cell structure in which the unit pore size is set to one.

As the porosity decreases or the solid volume fraction increases, the window sizes decrease, leading a closed-cell foam when $\phi = \phi_s$. However, due to the morphology complexity of real foam samples with high solid volume fraction, an accurate measurement of the critical solid volume fraction becomes challenging. Langlois et al. [17] suggested that $\phi_s = 0.32$ for the bcc structure, and $\phi_s \approx 0.38$ for real monodisperse foam samples (characterized by pores of uniform size). A common value found in the literature for disordered foam is $\phi_s \approx 0.36$ [19]. An alternative way to estimate the critical solid fraction ϕ_s of a real foam sample is available when both the open porosity ϕ and the tortuosity α_{∞} are known. In this case, the equation (5) can be applied with $\alpha_{\infty}^* = \alpha_{\infty}$. The estimated critical solid volume fraction ϕ_s is then employed to calculate the normalized transport parameters.

The equivalent Kelvin-cell pore sizes for each transport parameter of a real foam sample can be calculated by combining the normalized transport parameters of a Kelvin-cell

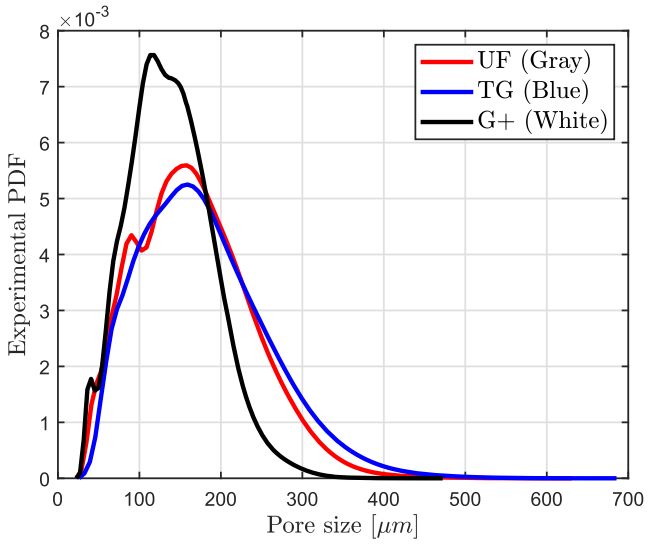

Figure 3. Experimental probability density functions of three melamine foams characterized from SEM images.

structure with the measured transport parameters, assuming they are available:

$$D_{k_0} = \left(k_0^{\exp}/k_0^*\right)^{0.5}, \tag{6}$$

$$D_{k_0'} = \left(k_0'^{\exp}/k_0'^*\right)^{0.5}, \tag{7}$$

$$D_{\Lambda} = \Lambda^{\exp}/\Lambda^*, \tag{8}$$

$$D_{\Lambda'} = \Lambda'^{\exp}/\Lambda'^*. \tag{9}$$

The superscript "exp" denotes experimental values. Note that $D_{\mathcal{TP}}$ is the size of the Kelvin cell for which the simulated transport parameter ($\mathcal{TP}$) matches the experimentally measured transport parameter. If an open-cell foam is monodisperse, the Kelvin cell constitute an adapted representation of the structure for simulating the acoustic behavior and therefore, it is expected that $D_{k_0} \approx D_{k_0'} \approx D_{\Lambda} \approx D_{\Lambda'}$. $D_{\mathcal{TP}}$ also describes an average pore size D of the real foam. Otherwise, the studied foam can no longer be considered as being monodisperse.

Now, we apply the proposed calculations to three commercially available melamine foams, namely UF (Gray), TG (Blue), and G+ (White). Visual inspection under SEM images reveals that these melamine foams do not exhibit membranes at all or only residual ones, as depicted in Figure 1. These lightweight foams present open porosity values very close to one (UF, $\phi = 0.992 \pm 0.005$; TG, $\phi = 0.988 \pm 0.005$; and G+, $\phi = 0.985 \pm 0.004$, the open porosity ϕ was measured by the pressure/mass method [20]). To collect microstructure information, we analyzed several SEM images (see Appendix). The pore size was provided by averaging over the semi-axis of an ellipse superimposed on the polyhedron forming the pore structure of the foam network (see inset of Fig. 1). Based on at least

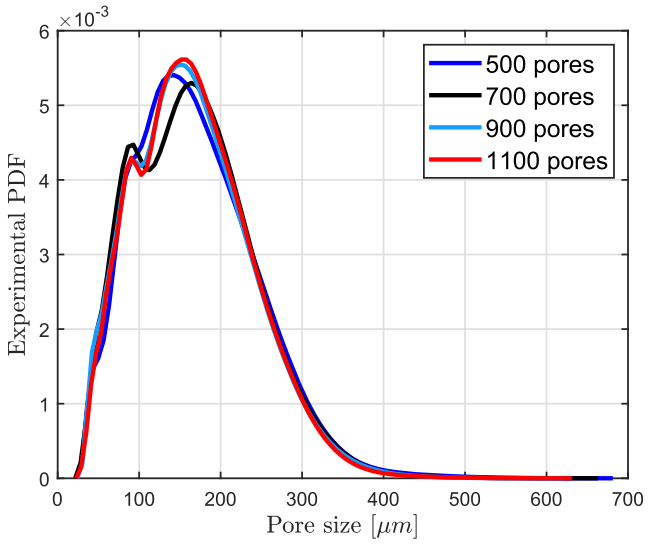

Figure 4. Experimental probability density functions of UF melamine foam for several number of detected pores.

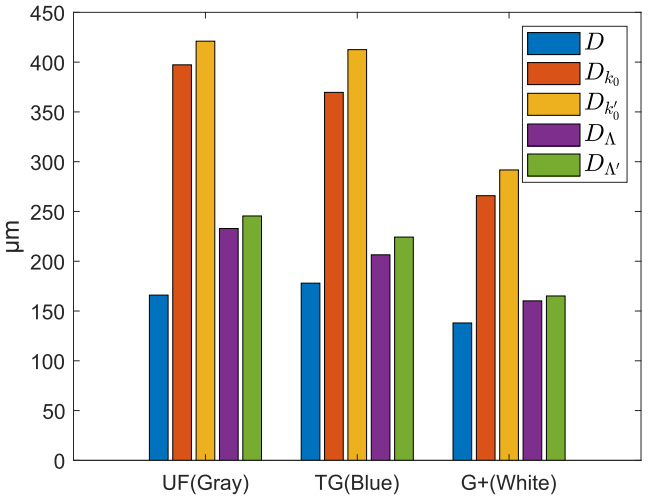

Figure 5. The average pore size D characterized by SEM-image analysis and the equivalent Kelvin-cell pore sizes $D_{\mathcal{TP}}$ calculated from equations (6) to (9) for three melamine foams.

1200 detected pores for each type of melamine foam, the average pore size (D) and its standard deviation (σ_D) were estimated. Additionally, a measure of the pore size polydispersity, specified by the coefficient of variation $C_D = \sigma_D/D$ was also considered.

The experimental probability density functions of the pore sizes derived from SEM images are displayed in Figure 3. It can be observed that all three melamine foams exhibit the pore size polydispersity ranging approximately between 50 µm and 500 µm. While the pore size distributions of the UF and TG melamine foams are found to be similar to each other, that of the G+ is narrower and presents a higher peak, indicating that the G+ foam is less polydisperse in pore size compared to UF an TG. The differences in the pore size distribution are attributed to variations in the manufacturing process (proportions of the chemical agents, catalysts, and temperature). Additionally, the convergence of the pore size distribution with respect to the number of pores was studied. An example of this analysis is provided for foam sample UF (Fig. 4). Interestingly, the results of this analysis show that convergences are reached from about 500 pores.

In Figure 5, we compare the average pore size D characterized by SEM-image analysis with the equivalent Kelvin-cell pore sizes $D_{\mathcal{TP}}$ calculated from equations (6)–(9), for three melamine foams under study. When doing so, the experimental transport parameters $\mathcal{TP}^{\text{exp}}$ introduced throughout equations (6)–(9) were obtained by the indirect characterization method [8, 9] (Tab. 1). From the simulation perspective, it is evident from Figure 5 that the equivalent Kelvin-cell pore sizes $D_{\mathcal{TP}}$ vary with the considered transport parameters. Another striking feature of this figure is that the average pore size D as mesured from SEM images is consistently smaller than the equivalent Kelvin-cell pore sizes determined from the top-down approach, whatever the considered melamine foam. This suggests that the all three studied foams are polydisperse, and that the average pore size is not an appropriate microstructural descriptor to adequately represent a polydisperse foam. Consequently, Kelvin-cell models with a single pore size, used for simulating the acoustic behavior of open-cell foams, are not appropriate representative volume elements of the three melamine foams investigated in this work.

Further important remarks can be drawn from the analysis of the results of Figure 5. First, the hierarchy between the equivalent pore sizes $D_{k'_0} \geq D_{k_0} \geq D_{\Lambda'} \geq D_\Lambda$ is always respected. As discussed earlier, equality is achieved only if the foams are monodispersed and the average pore size adequately represents the foam material. In fact, previous studies have demonstrated that for all porous microgeometries, the following relationships between transport parameters are necessarily valid, $k_0^{'} \geq k_0$ [21] and $\Lambda' \geq \Lambda$ [5] ($k_0^{'} = k_0$ and $\Lambda' \geq \Lambda$ only for tubes of constant cross-section shape, with the analytical relation $k_0 = \phi\Lambda^{'2}/8$). This evidence is enhanced by our findings suggesting that the ratios k'_0/k_0 and Λ'/Λ in melamine foams are greater than those found in monodisperse foams. Second, two principal groups of equivalent pore sizes $D_{\mathcal{TP}}$ appear, $D_{k'_0}$ and D_{k_0} on the one side, $D_{\Lambda'}$ and D_Λ on the other side, with a strong contrast between the values of these two groups. We note that the first group of equivalent pore sizes ($D_{k'_0}$, D_{k_0}) correspond to low-frequency transport parameters, and the second group of equivalent pore sizes ($D_{\Lambda'}$, D_Λ) correspond to high-frequency transport parameters. This observed contrast may be explained by the random microstructure's influence [22] on the visco-thermal dissipation mechanism of the sound propagation in porous media. This dissipation is depending on the viscous boundary layer δ_v, which diminishes with increasing angular frequency ω. Indeed, a real porous material like melamine foam consists of a network of randomly distributed pores with a random size distribution. In the low frequency behavior ($\omega \to 0$), the viscous boundary layer δ_v is large and the viscous fluid flows predominantly through the largest channels. Consequently, the effect of small pores in the microstructure network is

Table 1. Macroscopic parameters parameters of melamine foams: Comparison between characterization [8, 9], mono-sized model by Perrot et al. [13], 3-parameter model by Horoshenkov et al. [26] and poly-sized model (this work).

Foam	D (μm)	C_D (–)	k_0 ($\times 10^{-10}$ m^2)	k'_0 ($\times 10^{-10}$ m^2)	Λ (μm)	Λ' (μm)	α_∞ (–)
UF (Gray)							
Characterization	166	0.41	31.47 ± 3.69	75 ± 12	141 ± 14	298 ± 104	1.06 ± 0.03
Mono-sized model	397		31.47	67	241	450	1.03
3-parameter model			1.01	12.55	48.31	111.86	2.316
Poly-sized model			21.76	73.15	124.12	243.89	1.03
TG (Blue)							
Characterization	178	0.42	27.24 ± 1.89	72 ± 13	125 ± 15	254 ± 71	1.07 ± 0.04
Mono-sized model	369		27.24	58	224	419	1.03
3-parameter model			1.21	13.54	51.75	115.69	2.23
Poly-sized model			26.38	89.31	134.36	264.53	1.03
G+ (White)							
Characterization	138	0.36	14.09 ± 0.71	36 ± 6	97 ± 12	187 ± 12	1.08 ± 0.05
Mono-sized model	265		14.09	30	161	301	1.03
3-parameter model			1.11	7.94	45.14	86.95	1.926
Poly-sized model			11.62	37.37	98.62	191.99	1.03

negligible and the visco-thermal effects at low frequencies require a large equivalent pore size. On the other hand, in the high-frequency behavior ($\omega \to \infty$), the influence of the viscous boundary layer δ_v diminishes and the fluid behaves as a perfect or inviscid one, able to penetrate all pores of the network including the smallest pores. This emphasizes the significance of smaller pores at high frequencies, elucidating why the visco-thermal effects at high acoustical frequencies necessitates a representative pore with a smaller size. The higher the polydispersity C_D, the larger the contrast between the low-frequency and high-frequency transport parameters and the corresponding equivalent pore diameters.

3 Application of micro-macro models to melamine foams

In our perivious work [23], we developed a numerical approach to simulate the acoustic properties of high porous polydisperse foams, which also include thin membranes. This approach is based on a homogenization approach and an advanced Laguerre tessellation, wherein the pore size distribution is described by the log-normal probability law with parameters such as the average size D and the the pore size polydispersity C_D. Additionally, the membrane content is characterized by the proportion of open membranes x_o and the aperture ratio τ_o of these membranes. It is important to note that the aperture ratio of an open membrane is defined as the ratio of the area of the opening part to the total area of the considered membrane (see Fig. 2 of Ref. [23]). In spite of the fact that the ligament effect was not considered, an application to a real polydisperse polyurethane foam showed the reliability of this approach. In the specific scenario resembling an open-cell foam configuration where all membranes are open with an identical aperture ratio (τ_o is set to a constant, and $x_o = 1$), the simulations yield the following results (see Ref. [24] for more details:

$$\frac{D_{k_0}}{D} = 5.688\left(e^{0.9548C_D^2} - 1\right) + 1, \tag{10}$$

$$\frac{D_{k'_0}}{D} = 28.870\left(e^{0.3023C_D^2} - 1\right) + 1, \tag{11}$$

$$\frac{D_{\Lambda}}{D} = 6.001\left(e^{0.2283C_D^2} - 1\right) + 1, \tag{12}$$

$$\frac{D_{\Lambda'}}{D} = 9.919\left(e^{0.1757C_D^2} - 1\right) + 1. \tag{13}$$

Importantly, the macroscopic transport parameters of a polydisperse foam with a given open porosity ϕ can then be deduced from the corresponding equivalent pore size $D_{\mathcal{TP}}$ and the normalized transport parameters $\mathcal{TP}^*$ of a Kelvin-cell structure, as provided by Langlois et al. [17], with the analytical expressions described by equations (1)–(5):

$$k_0 = D_{k_0}^2 k_0^*, \tag{14}$$

$$k'_0 = D_{k'_0}^2 k_0'^*, \tag{15}$$

$$\Lambda = D_\Lambda \Lambda^*, \tag{16}$$

$$\Lambda' = D_{\Lambda'} \Lambda'^*, \tag{17}$$

$$\alpha_\infty = \alpha_\infty^*. \tag{18}$$

Therefore, for an open-cell foam without membranes, the aperture ratio τ_o was considered to be close to one. Assuming the open porosity is known from measurements, the developed structure-property relationships can be utilized to determine the transport parameters from the morphological features derived by SEM-image analysis, including the average pore size D and the polydispersity C_D. Moreover,

the sound absorption coefficient at normal incidence is estimated using the JCAL model [5–7], wherein the obtained transport parameters serve as inputs.

It is also worth recalling here the so-called Horoshenkov's 3-parameter model for comparison purposes, designed for materials with pore size distributions close to log-normal [25, 26]. From three independent and measurable parameters including the open porosity ϕ, the median pore radius $\bar{s}$, and the standard deviation σ_s of the pore radius distribution taken on the log-normal scale [$-\log_2(s)$ with s denotes the pore radius], the 3-parameter model provides relations to compute the remaining parameters of the JCAL model:

$$\alpha_\infty = e^{4(\sigma_s \log 2)^2}, \tag{19}$$

$$k_0 = \frac{\phi \bar{s}^2}{8\alpha_\infty} e^{6(\sigma_s \log 2)^2}, \tag{20}$$

$$k_0' = \frac{\phi \bar{s}^2}{8\alpha_\infty} e^{-6(\sigma_s \log 2)^2}, \tag{21}$$

$$\Lambda = \bar{s} e^{-5/2(\sigma_s \log 2)^2}, \tag{22}$$

$$\Lambda' = \bar{s} e^{3/2(\sigma_s \log 2)^2}. \tag{23}$$

The results of these models including our polydisperse (poly-sized) model and the 3-parameter one for the transport parameters are presented in Table 1, while Figure 6 illustrates the sound absorption coefficients at normal incidence of the three melamine foams investigated in this work with a thickness of 30 mm. Additionally, we compare these results with those obtained using the simplified top-down model introduced by Perrot et al. [13]. We recall that, in this mono-sized model, the foams are assumed to be monodispersed, and the pore size is adjusted so that the calculated permeability and porosity matched the characterized one.

As shown in Table 1, both the mono-sized and poly-sized models yield acceptable values of the tortuosity from an acoustic perspective, typically around 1.05 for open-cell foams [27–29]. For the remaining transport parameters, it is evident that, apart from k_0, which is an input parameter obtained from experiments, the values calculated with the mono-sized model are generally overestimated when compared with the characterized ones. Specifically, this simplified model leads to an overestimation of the viscous and thermal characteristic lengths by a factor of two. Obviously, this discrepancy arises because the mono-sized model neglects the effect of polydispersity in using only an equivalent pore size to simulate all macroscopic parameters. Consequently, the estimated average pore sizes (derived from the measured permeability and open porosity) deviates significantly from that characterized by SEM images.

The 3-parameter model results in a significant overestimation of the tortuosity α_∞ and an underestimation of the remaining transport parameters. This observation provides

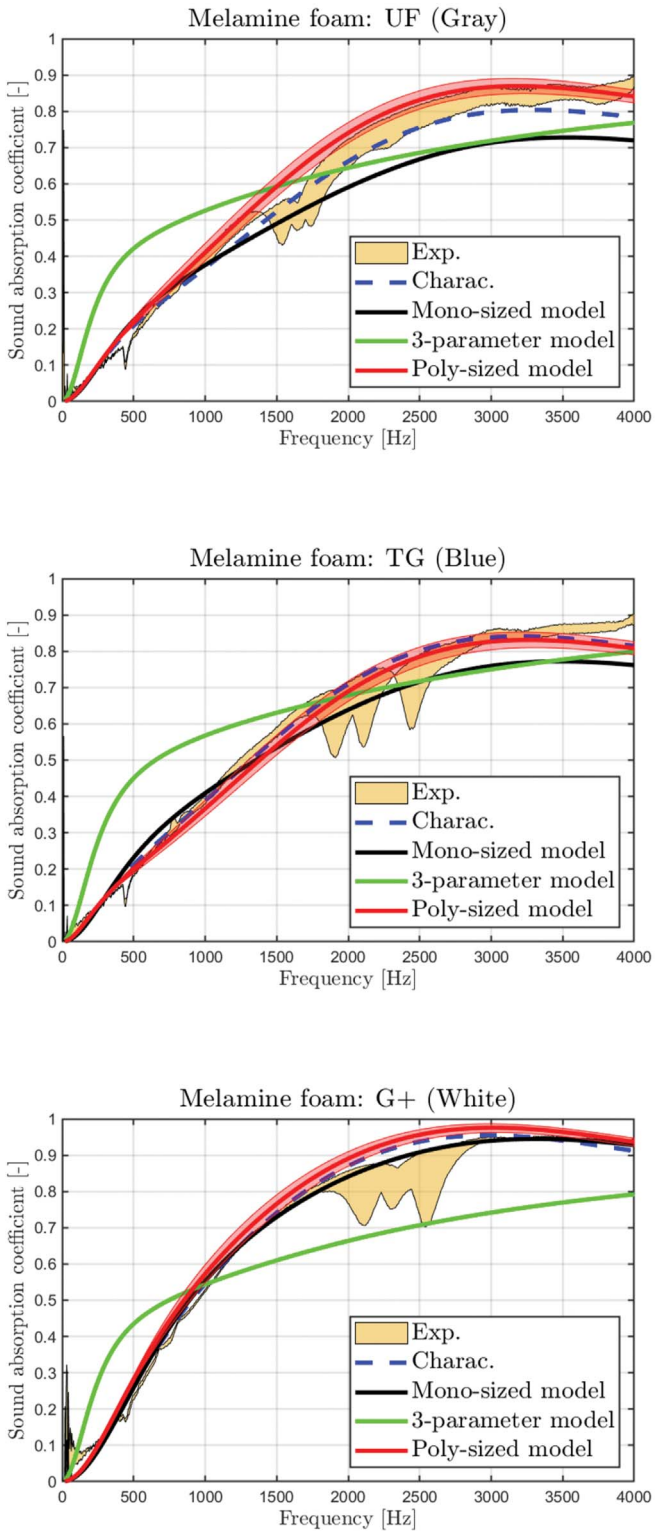

Figure 6. Sound absorbing coefficients at normal incidence of 30 mm thickness melamine foam samples: Comparison between measurements (orange filled zone), characterization [8, 9] (blue dashed line), mono-sized model [4] (black line), 3-parameter model [26] (green line), and poly-sized model [this work] (red filled zone with full line). The poly-sized model curves are calculated by using the computed macroscopic parameters (Tab. 1), uncertainties determined by considering an error of 5% on the measured pore size D.

valuable insight into the applicability of the 3-parameter model. While effective in fitting experimental data for specific material types, it may prove inadequate for open-cell foams. We interpret this limitation of the model from the fact that it relies on the assumption of an infinite sequence of continuous and instantaneous cross-sectional changes, a condition that does not hold for such materials.

Incorporating the effect of polydispersity into our poly-sized model leads to a more accurate estimation of the transport parameters for melamine foams. As a result, the predictions of the sound absorption coefficient at normal incidence by a polydisperse model closely approximate the experimental results (as shown in Fig. 6). By contrast, the 3-parameter model fails to globally predict the sound absorbing behavior. For UF and TG foams exhibiting relatively high polydispersity, the mono-sized model fails to accurately simulate the acoustic behavior (particularly in the high-frequency range). However, for the G+ foam, this model predicts accurately the sound absorption (even more precisely than the polydisperse model). This is because the G+ foam is approximately monodisperse (Fig. 3, black curve), and the mono-sized model directly utilizes the measured viscous permeability k_0 as an input (one of the most influential parameters on the acoustic properties). In this case, C_D might not be the most appropriate morphological descriptor of the polydispersity (0.36 is numerically close to 0.41 but the corresponding distributions are fairly different). By contrast, the input parameters of the poly-sized model are purely morphological, and characterized by SEM-image analysis (the average pore size D and the polydispersity C_D) without any adjusted parameter. Note that the peaks observed around 1600 Hz for UF foam (and around 2000–2500 Hz for both TG foam and G+ foam) in the experimental sound absorption curves are not addressed from a modelling point of view in this study. Indeed, these peaks are attributed to frame resonance in the acoustic tube experiment and can be mitigated by adding thin nails or needles to the foam samples. However, in order to avoid possible modification of the foam structure, a post-processing choice was done in this work, which consisted in discarding the frequency range at which resonance occurs from the analysis for each sample. The frame resonance phenomenon does not significantly impact the acoustic behavior outside these local frequency ranges [9].

As a whole, a minor difference can be observed between experiments and our poly-sized computations for both the transport parameters and sound absorption coefficient at normal incidence. The small discrepancies could be explained by several factors: (i) a potential bias in the characterized pore size (2D-image measurements); (ii) the assumption of a log-normal probability law for the pore size distribution; (ii) the ligament's cross-section shape is not considered in the structure-property relationships described through equations (10)–(13) (originally developed for membrane-based foams, Ref. [23]). Nevertheless, our poly-sized model demonstrated the importance of accounting for microstructure polydispersity in acoustic simulations for real melamine foams.

4 Conclusion

This study investigated the influence of pore size distribution on the acoustic properties of three commercially available melamine foams. By utilizing measured transport parameters, a top-down approach was employed to determine a single equivalent pore size corresponding to each transport parameter. The differences observed in these equivalent pore sizes indicate that the mono-sized model is not suitable for these materials. Accounting for macro-scale information through an overall picture of transport parameters highlighted the polydisperse nature of the microstructure and its impact on the acoustic behavior of melamine foams. The polydispersity was confirmed through experimental evidence at the micro-scale from the analysis of SEM images. Furthermore, the measurements collected at micro-scale (average pore size and its standard deviation) served as input data to determine the transport and sound absorbing behavior of melamine foam samples using structure-property relationships available for open cell microstructures (without any adjusted parameter). This work emphasized the importance of accounting for the polydispersity of melamine foams to obtain, in such open-cell and high-porosity foams, an accurate and consistent understanding of their microstructure and transport properties.

1. A unified set of formula for the rapid prediction of transport properties from morphological parameters (ϕ, D, CD), valid for open-cell foam without membranes, has been derived.
2. For high-porosity open-cell foams, the transport parameters obtained through direct measurements (k_0, Λ, Λ') enable access to microstructure parameters (D, C_D) (see Ref. [24]).
3. Further research is required on polydisperse materials, including systems with polydispersity understood as a new optimization lever (experimental validation of the morphological optimum, extension to elastic and thermal properties, effect of variability).

Acknowledgments

Dengke Li received a grant from the Chinese Scholarship Council under No CSC 201604910577 to work on a short range research project at the MSME UMR 8208 CNRS laboratory in the framework of a joint PhD together with the Key Laboratory of Noise and Vibration Research from the Institute of Acoustics of the Chinese Academy of Sciences. The work from Ziming XIONG was partially funded by TREVES CERA APS under reference contract No 2017-00143. Porosity measurements were performed at TREVES CERA APS with an experimental support from both Anders LINDBERG and Lei LEI whose support are gratefully acknowledged. We also acknowledge the technical assistance provided by Rémy PIRES BRAZUNA (SEM images) from the Institut de Chimie des Matériaux Paris-Est (ICMPE, France).

This work was also supported by the French National Research Agency (ANR-21-PRRD-0001-01) as part of the France Relance project under the Centre National de la Recherche Scientifique research collaborative agreement (REF CNRS number 247060) between CNRS, Université Gustave Eiffel, Université

Paris-Est Créteil Val-de-Marne and TREVES, Products, Services and Innovation Group.

This work is also supported by the National Natural Science Foundation of China (No. 52205269).

Conflicts of interest

All authors declare that they have no conflicts of interest.

Data availability statement

The data are available from the corresponding author on request.

References

1. Y. Imashiro, S. Hasegawa, T. Matsumoto: Melamine resin foam, United States Patent 5413853, 1995.
2. J. Plateau: Statique expérimentale et théorique des liquides soumis aux seules forces moléculaires, vol. 2, Gauthier-Villars, Paris, 1873.
3. V. Magnenet, R. Rahouadj, P. Bacher, C. Cunat: Inelastic constitutive relations for foamed materials: a statistical approach and its application to open-cell melamine, Mechanics of Materials 40, 9 (2008) 673–684.
4. K.A. Brakke: The surface evolver, Experimental Mathematics 1, 2 (1992) 141–165.
5. D.L. Johnson, J. Koplik, R. Dashen: Theory of dynamic permeability and tortuosity in fluid-saturated porous media, Journal of Fluid Mechanics 176 (1987) 379–402.
6. Y. Champoux, J.-F. Allard: Dynamic tortuosity and bulk modulus in air-saturated porous media, Journal of Applied Physics 70, 4 (1991) 1975–1979.
7. D. Lafarge, P. Lemarinier, J.-F. Allard, V. Tarnow: Dynamic compressibility of air in porous structures at audible frequencies, Journal of the Acoustical Society of America 102, 4 (1997) 1995–2006.
8. R. Panneton, X. Olny: Acoustical determination of the parameters governing viscous dissipation in porous media, Journal of the Acoustical Society of America 119, 4 (2006) 2027–2040.
9. X. Olny, R. Panneton: Acoustical determination of the parameters governing thermal dissipation in porous media, Journal of the Acoustical Society of America 123, 2 (2008) 814–824.
10. H. Utsuno, T. Tanaka, T. Fujikawa, A.F. Seybert: Transfer function method for measuring characteristic impedance and propagation constant of porous materials, Journal of the Acoustical Society of America 86, 2 (1989) 637–643.
11. N. Geebelen, L. Boeckx, G. Ve, W. Lauriks, J.F. Allard, O. Dazel: Measurement of the rigidity coefficients of a melamine foam, Acta Acustica united with Acustica 93 (2007) 783–788.
12. P. Göransson, R. Guastavino, N.E. Hörlin: Measurement and inverse estimation of 3D anisotropic flow resistivity for porous materials, Journal of Sound and Vibration 327, 3–5 (2009) 354–367.
13. C. Perrot, F. Chevillotte, M. Tan Hoang, G. Bonnet, F.-X. Bécot, L. Gautron, A. Duval: Microstructure, transport, and acoustic properties of open-cell foam samples: Experiments and three-dimensional numerical simulations, Journal of Applied Physics 111, 1 (2012) 14911.
14. T.G. Zieliński, R. Venegas, C. Perrot, M. Červenka, F. Chevillotte, K. Attenborough: Benchmarks for microstructure-based modelling of sound absorbing rigid-frame porous media, Journal of Sound and Vibration 483 (2020) 115441.
15. W. Thomson: LXIII. On the division of space with minimum partitional area, The London, Edinburgh, and Dublin Philosophical Magazine and Journal of Science 24, 151 (1887) 503–514.
16. N.J. Mills: The wet Kelvin model for air flow through open-cell polyurethane foams, Journal of Materials Science 40, 22 (2005) 5845–5851.
17. V. Langlois, A. Kaddami, O. Pitois, C. Perrot: Acoustics of monodisperse open-cell foam: an experimental and numerical parametric study, Journal of the Acoustical Society of America 148, 3 (2020) 1767–1778.
18. B.P. Semeniuk, E. Lundberg, P. Göransson: Acoustics modelling of open-cell foam materials from microstructure and constitutive properties, Journal of the Acoustical Society of America 149, 3 (2021) 2016–2026.
19. W. Drenckhan, S. Hutzler: Structure and energy of liquid foams, Advances in Colloid and Interface Science 224 (2015) 1–16.
20. Y. Salissou, R. Panneton: Pressure/mass method to measure open porosity of porous solids, Journal of Applied Physics 101, 12 (2007) 124913.
21. M. Avellaneda, S. Torquato: Rigorous link between fluid permeability, electrical conductivity, and relaxation times for transport in porous media, Physics of Fluids A: Fluid Dynamics 3, 11 (1991) 2529–2540.
22. N. Martys, E.J. Garboczi: Length scales relating the fluid permeability and electrical conductivity in random two-dimensional model porous media, Physical Review: B Condensed Matter 46, 10 (1992) 6080–6090.
23. C.T. Nguyen, V. Langlois, J. Guilleminot, F. Detrez, A. Duval, M. Bornert, P. Aimedieu, C. Perrot: Polydisperse solid foams: multiscale modeling and simulations of elasto-acoustic properties including thin membrane effects, International Journal of Solids and Structures 249 (2022) 111684.
24. C.T. Nguyen, V. Langlois, J. Guilleminot, A. Duval, C. Perrot: Effect of pore size polydispersity on the acoustic properties of high-porosity solid foams, Physics of Fluids 36, 4 (2024) 047101.
25. K.V. Horoshenkov, J.-P. Groby, O. Dazel: Asymptotic limits of some models for sound propagation in porous media and the assignment of the pore characteristic lengths, Journal of the Acoustical Society of America 139, 5 (2016) 2463–2474.
26. K.V. Horoshenkov, A. Hurrell, J.-P. Groby: A three-parameter analytical model for the acoustical properties of porous media, Journal of the Acoustical Society of America 145, 4 (2019) 2512–2517.
27. O. Doutres, N. Atalla, K. Dong: Effect of the microstructure closed pore content on the acoustic behavior of polyurethane foams, Journal of Applied Physics 110, 6 (2011) 64901.
28. O. Doutres, N. Atalla, K. Dong: A semi-phenomenological model to predict the acoustic behavior of fully and partially reticulated polyurethane foams, Journal of Applied Physics 113, 5 (2013) 54901.
29. N. Kino, G. Nakano, Y. Suzuki: Non-acoustical and acoustical properties of reticulated and partially reticulated polyurethane foams, Applied Acoustics 73, 2 (2012) 95–108.

Appendix

Protocol of preparation of samples prior to the acquisition of SEM images

For non-conductive materials like melamine foams, a high performance metallizer by cathodes puttering was used, coupled with a magnetron source (Cressington sputter

coater 208HR); which made it possible to deposit a conductive film of a few nanometers (controlled by aquartz probe, here a Cressington MTM20) on the surface of the samples. To verify the homogeneity of the microstructure, specifically in terms of pore diameters, four specimens with dimensions of 3 mm were taken randomly from different locations of the studied panels (two samples extracted from the horizontal planes and two samples taken from the vertical planes). On each extracted specimen, SEM images were then acquired to fully scan the apparent surfaces. The degree of anisotropy was assessed by controlling the value of the ratio $D_v = D_h$, where D_v (respectively D_h) is the average diameter of detected pores in the vertical plane (respectively in the horizontal plane). In practice, this ratio is found to be typically smaller than 1.15 for all samples, so that the effect of geometric anisotropy is neglected in this work.

Cite this article as: Nguyen CT. Li D. Xiong Z. He M. Gautron L, et al. 2024. Structure-property relationships of polydisperse open-cell foams: application to melamine foams. Acta Acustica, **8**, 54. https://doi.org/10.1051/aacus/2024046.